PERGAMON

International Journal of Heat and Mass Transfer 46 (2003) 323–332

International Journal of HEAT and MASS TRANSFER

www.elsevier.com/locate/ijhmt

# Linear stability of cold water layer saturating an anisotropic porous medium—effect of confinement

A. Mahidjiba, L. Robillard *, P. Vasseur

*Department of Mechanical Engineering, Ecole Polytechnique, University of Montreal, CP 6079, Succ. 'Down Town', Montreal, PQ, Canada H3C 3A7*

Received 3 August 2001; received in revised form 17 June 2002

**Abstract**

The linear stability analysis is applied to a horizontal porous layer saturated with water in the neighborhood of 4 °C. The porous layer considered is two-dimensional and anisotropic in permeability with principal axes arbitrarily oriented. The onset of convection depends on parameters such as the aspect ratio $A$, the permeability ratio $K^*$, the orientation angle, $\theta$ of the principal axes and the inversion parameter, $\gamma$. The relevant linearized equations are solved with the aid of Galerkin and finite element methods. Results for the case of an infinite layer indicate that the presence of a stable layer near the upper boundary for $\gamma < 2$ changes drastically the critical Rayleigh number and that an asymptotic situation is reached when $\gamma \leqslant 1$. For that asymptotic situation, and with $\theta = 0°$ or 90°, the incipient flow field consists of primary convective cells near the lower boundary with superposed layers of secondary cells. For $0° < \theta < 90°$, primary and secondary cells coalesce to form obliquely elongated cells.


## 1. Introduction

A limited number of studies was devoted in the past to the instability of a horizontal anisotropic porous layer saturated by cold water. For this situation, the relation between the density of the fluid and the temperature is nonlinear and the density of the fluid reaches a maximum value.

The onset of convection of cold water has been considered in the past by Veronis [1] and later by Musman [2] and Moore and Weiss [3]. When the 4 °C isotherm lies between the upper and lower boundaries, there exists in pure conduction an upper stable layer superposed to a lower unstable one. In their studies, these authors have used a Rayleigh number based on the depth of the unstable layer and on the difference of density across that layer. Other publications such as those of Poulikakos [4] and more recently, Mamou et al. [5] concern the instability of an isotropic porous medium saturated with cold water. The instability of an anisotropic porous layer of infinite extent with arbitrary oriented principal axes was investigated analytically by Tyvand and Storesletten [6] for the classical case of a linear density–temperature relationship and by Straughan and Walker [7] for the cold water case. Those last authors have used both the linear stability and the nonlinear energy stability analyses in their investigation.

Recently, Mahidjiba et al. [8] studied the effect of lateral confinement on the threshold of an anisotropic porous layer with arbitrary oriented principal axes. A subsequent publication, also by Mahidjiba et al. [9], deals with the anisotropic porous layer of infinite extent saturated by cold water, the principal axes being limited to horizontal/vertical orientations. The present paper concerns the anisotropic porous layer saturated with cold water with arbitrary orientation of the principal axes. The effect of confinement is also considered.

* Corresponding author. Tel.: +1-514-340-4238/4711/4154; fax: +1-514-340-3240/5917.

*E-mail address:* robillard@meca.polymtl.ca (L. Robillard).

*URL:* http://www.meca.polymtl.ca/convection.

0017-9310/03/$ - see front matter 
PII: S0017-9310(02)00262-4

**Nomenclature**

| | |
|---|---|
| $A$ | aspect ratio, $L'/H'$ |
| $A_m$ | modified aspect ratio, Eqs. (7a) and (7b) |
| $H'$ | overall height of the layer |
| $h'_{max}$ | height of the unstable layer |
| $k$ | thermal conductivity of the saturated porous medium |
| $K^*$ | permeability ratio, $K_2/K_1$ |
| $L'$ | width of the porous layer |
| $R$ | Darcy Rayleigh number, $K_2 g\beta'\Delta T'^2 H'/(\alpha\nu)$ |
| $R_m$ | modified Darcy Rayleigh number, Eqs. (7a) and (7b) |
| $t$ | dimensionless time, $t'/(\sigma H'^2/\alpha)$ |
| $\Delta T'$ | temperature difference based on the overall depth of the layer, $T'_U - T'_L$ |
| $T'_{max}$ | temperature corresponding to the density $\rho_{max}$, ($T'_{max} = 4$ °C) |
| $(x, y)$ | dimensionless coordinate system, $x'/H'$, $y'/H'$ |
| $(u, v)$ | dimensionless velocity terms, $u'/(\alpha/H')$, $v'/(\alpha/H')$ |

*Greek symbols*

| | |
|---|---|
| $\alpha$ | thermal diffusivity, $k/(\rho_{max}C)_f$ |
| $\beta$ | thermal expansion coefficient, Eq. (8), °C$^{-2}$ |
| $\beta_1$ | coefficient, Eq. (1), °C$^{-2}$ |
| $\gamma$ | inversion parameter, $2(T'_{max} - T'_L)/\Delta T'$ |
| $\theta$ | orientation angle |
| $\lambda$ | wavelength |
| $\overline{\lambda}$ | eigenvalue |
| $\sigma$ | heat capacity ratio, $(\rho_m C)_p/(\rho_m C)_f$ |
| $\nu$ | kinematic viscosity of fluid |
| $\rho$ | density of fluid |
| $\rho_{max}$ | maximum density |
| $(\rho_{max}C)_f$ | heat capacity of fluid |
| $(\rho_{max}C)_p$ | heat capacity of saturated porous medium |
| $\Psi$ | dimensionless stream function, $\Psi'/\alpha$ |

*Subscripts*

| | |
|---|---|
| c | critical value at incipient convection |
| m | modified value |

## 2. Mathematical formulation

The problem under consideration is illustrated in Fig. 1. It consists of a two-dimensional horizontal porous layer, anisotropic in permeability, with principal axes defined by extremum permeabilities $K_1$ and $K_2$ arbitrary oriented, according to the angle $\theta$. Uniform temperatures $T'_L$ and $T'_U$ are imposed on the horizontal boundaries. The two vertical boundaries are subject either to adiabatic or periodic conditions (those last conditions to be defined later), according to the type of layer (confined or unconfined) considered. When, $T'_{max}$ the temperature corresponding to the maximum density of water, is between $T'_L$ and $T'_U$, a pure conduction density distribution takes the form given in Fig. 1. The vertical position of the maximum density defines a separating line between a lower unstable region and a superposed stable one. The saturated porous layer is assumed to follow the Darcy law. The fluid density varies with temperature according to a parabolic relationship of the form

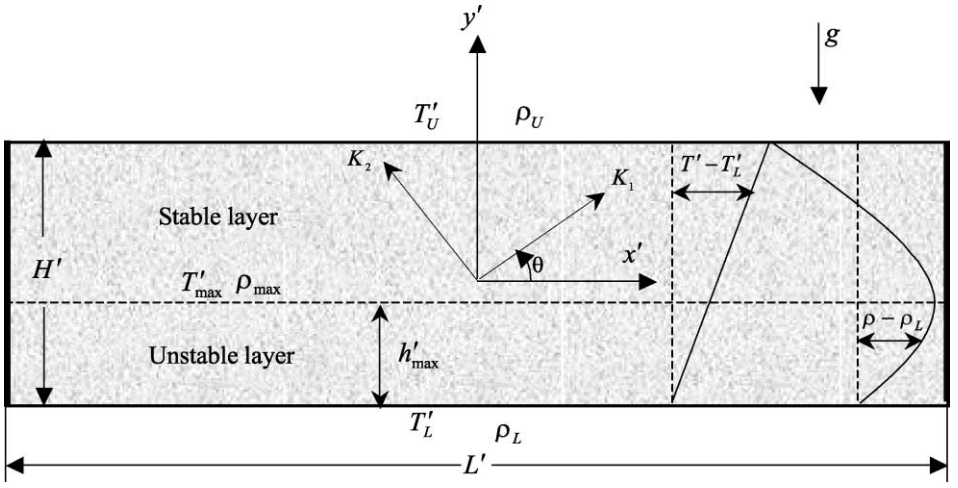


Fig. 1. Geometry of the physical problem.

$$\rho = \rho_{\max}\lfloor 1 - \beta_1 (T' - T'_{\max})^2 \rfloor \quad (1)$$

with $T'_{\max} = 3.98$ °C and $\beta_1 = 8 \times 10^{-6}$ °C$^{-2}$. The resulting relation was found to hold to within 4% over the range 0–8 °C, according to Moore and Weiss [3].

Using, $H'$, $\alpha = k/(\rho_{\max} C)_f$, $\alpha/H'$, $t'/(\sigma H'^2/\alpha)$ and $\Delta T' = T'_U - T'_L$ as respective scales for length, stream function, velocity, time and temperature, the dimensionless equations for momentum and energy [8,9] are

$$a\frac{\partial^2 \Psi}{\partial x^2} + b\frac{\partial^2 \Psi}{\partial x \partial y} + c\frac{\partial^2 \Psi}{\partial y^2} = R(\gamma - 2T)\frac{\partial T}{\partial x} \quad (2)$$

$$\frac{\partial T}{\partial t} + u\frac{\partial T}{\partial x} + v\frac{\partial T}{\partial y} = \frac{\partial^2 T}{\partial x^2} + \frac{\partial^2 T}{\partial y^2} \quad (3)$$

where $a = \cos^2\theta + K^* \sin^2\theta$, $b = (1 - K^*)\sin 2\theta$ and $c = \sin^2\theta + K^* \cos^2\theta$ and where the stream function $\Psi$ is related to the velocity by the usual relations $u = \partial\Psi/\partial y$ and $v = -\partial\Psi/\partial x$.

In the above equations, $R = K_2 g \beta_1 \Delta T'^2 H'/(\nu\alpha)$ is the Rayleigh number, $\gamma = 2(T'_{\max} - T'_L)/\Delta T'$, the inversion parameter and $K^* = K_2/K_1$, the permeability ratio. Together with the aspect ratio $A = L'/H'$ and the orientation angle $\theta$ defined in Fig. 1, they are the governing parameters of the present problem.

For the interpretation of the results, it is more appropriate to used a modified Rayleigh number $R_m$ and a modified aspect ratio $A_m$, both based on the depth $h'_{\max}$ of the unstable layer and on the difference of density $\Delta\rho_m$ across that layer. Thus the physical definition of the Rayleigh number remains the same,

$$R_m = \frac{K_2 g}{\alpha\nu}\frac{\Delta\rho_m}{\rho_{\max}} h'_{\max} \quad (4)$$

although its mathematical expression changes, according to the vertical position of the maximum density in pure conduction. For the maximum density between the two horizontal boundaries ($0 < \gamma \leqslant 2$), we have

$$h'_{\max} = H'(\gamma/2)$$
$$\frac{\Delta\rho_m}{\rho_{\max}} = \frac{\rho_{\max} - \rho_L}{\rho_{\max}} = \beta_1 (T'_{\max} - T'_L)^2 = \beta_1 [(\gamma/2)\Delta T']^2 \quad (5)$$

For the maximum density above the upper boundary $\gamma \geqslant 2$, we have

$$h'_{\max} = H'$$
$$\frac{\Delta\rho_m}{\rho_{\max}} = \frac{\rho_U - \rho_L}{\rho_{\max}} = -\frac{\rho_{\max} - \rho_U}{\rho_{\max}} + \frac{\rho_{\max} - \rho_L}{\rho_{\max}} \quad (6)$$

Eqs. (5) and (6) are used to define a modified Rayleigh number and a modified aspect ratio as

$$0 < \gamma \leqslant 2 \quad R_m = R(\gamma/2)^3 \quad A_m = A(\gamma/2)^{-1} \quad (7a)$$

$$\gamma \geqslant 2 \quad R_m = R(\gamma - 1) \quad A_m = A \quad (7b)$$

On one hand, with $\gamma \gg 2$, the quadratic term in $T$ of Eq. (2) becomes negligible and, since the thermal expansion coefficient $\beta$ used in linear convection is related to $\beta_1$ according to $\beta = 2\beta_1(T' - T'_{\max})$ (see [10]), we obtain

$$R_m \approx R\gamma = \frac{K_2 g \beta_1 \Delta T'^2}{\nu\alpha}(T'_{\max} - T'_L)H'$$
$$= -\frac{K_2 g \beta \Delta T'}{\nu\alpha} H' = -R_1 \quad (8)$$

$R_1$ being the standard Rayleigh number for linear convection. Eq. (8) represents one of the asymptotic limits of the results to be presented. On the other hand, there exists also, as it will be shown, another asymptotic limit for $\gamma \leqslant 1$, for which the (modified) Rayleigh number, as defined in (7a), remains constant. It is to be noted that both definitions of given in (7a) and (7b) coincide when $\gamma = 2$.

On all solid boundaries, hydrodynamic boundary conditions are $\Psi = 0$, while the thermal boundary conditions are

$$x = \pm A/2 \quad \partial T/\partial x = 0$$
$$y = 1/2 \quad T = 0$$
$$y = -1/2 \quad T = 1 \quad (9)$$

For the infinite layer, where the flow structure consists of periodic counterrotating cells, periodic boundary conditions in the $x$-direction are used to study the incipient convection, the aspect ratio $A$ being limited to one wavelength $\lambda$. Those periodic conditions are defined as $\phi(x, y) = \phi(x + \lambda_c, y)$, where $\varphi$ stands for any physical variable and $\lambda_c$ corresponds to the critical wavelength.

## 3. Linear stability analysis

In the present work, the threshold of convection is obtained numerically. The method has been described in the past by Mahidjiba et al. [8,9] and only a brief description is presented here. The following transformation is introduced

$$\Psi(x, y) = \Psi_R + \psi(x, y) \quad \text{and}$$
$$T(x, y) = T_R + \phi(x, y) \quad (10)$$

where $\Psi_R = 0$ and $T_R = y + 1/2$ correspond to the rest state and $\psi(x, y)$ and $\varphi(x, y)$ are the perturbed solutions resulting from the convective effects.

Assuming separability, the steady perturbed solution can be written as follows:

$$\psi(x, y) = \psi_0 F(x, y) \quad \text{and} \quad \varphi(x, y) = \varphi_0 G(x, y) \quad (11)$$

where the amplitudes $\psi_0$ and $\phi_0$ are small constants.

Substituting the rest-state solution and the small perturbations, Eqs. (10) and (11), into the governing

Eqs. (2) and (3) and discarding the second order terms involving the perturbations (at the beginning of convection, the amplitude $\psi_0$ and $\varphi_0$ are close to zero), the following linearized set of governing equations is obtained:

$$\psi_0\left(a\frac{\partial^2}{\partial x^2}+b\frac{\partial^2}{\partial x\partial y}+c\frac{\partial^2}{\partial y^2}\right)F=Rf(y)\phi_0\frac{\partial G}{\partial x} \tag{12}$$

$$-\psi_0\frac{\partial F}{\partial x}=\phi_0\left(\frac{\partial^2 G}{\partial x^2}+\frac{\partial^2 G}{\partial y^2}\right) \tag{13}$$

where $f(y)=\gamma-2y-1$.

The boundary conditions for $F$ are similar to those of $\Psi$, except for $y=1/2$ where $F$ takes the zero value. $G$ also follows the boundary conditions for $T$.

The finite element method is employed to solve the above set of equations. The details of this method were already mentioned in the articles by Mahidjiba et al. [8,9]. After calculation and rearrangement of the terms, we obtain the following discretized set of linear equations

$$\psi_0\lfloor K_\psi\rfloor\{F\}=R\varphi_0[B]\{G\}\quad\text{and}$$
$$\psi_0[L]\{F\}=\varphi_0[K]\{G\} \tag{14}$$

where $[B]$, $\lfloor K_\psi\rfloor$, $[K]$ and $[L]$ are $m\times m$ square matrices with $m=4N_n$, $N_n$ being the total number of nodes, defined as $N_n=(N_{ex}+1)(N_{ey}+1)$; $N_{ex}$ and $N_{ey}$ are the numbers of elements in $x$-direction and $y$-direction, respectively. The corresponding elementary matrices can be computed from the following integrals:

$$[B]^e=-\int_{\Omega^e}f(y)\frac{\partial N_j}{\partial x}N_i\,d\Omega^e$$
$$[K]^e=\int_{\Omega^e}\nabla N_j\cdot\nabla N_i\,d\Omega^e$$
$$[L]^e=\int_{\Omega^e}\frac{\partial N_j}{\partial x}N_i\,d\Omega^e$$
$$[K_\psi]^e=\int_{\Omega^e}\left(a\frac{\partial N_j}{\partial x}\frac{\partial N_i}{\partial x}+b\frac{\partial N_j}{\partial y}\frac{\partial N_i}{\partial x}+c\frac{\partial N_j}{\partial y}\frac{\partial N_i}{\partial y}\right)d\Omega^e \tag{15}$$

where $N_j(y)$ are either the Lagrange interpolation functions for a quadratic case or the Hermite interpolation functions for the cubic case; $\{F\}$ and $\{G\}$ are solution vectors of length $m$.

It is noted that boundary integrals, known as the natural boundary conditions, vanish for the homogeneous Dirichlet and Neumann boundary conditions. Eliminating $\varphi_0$ from Eq. (14), we obtain the following eigenvalue problem equation

$$\psi_0([E]-\bar{\lambda}[I])\{F\}=0\quad\text{with}\quad[E]=[K_\psi]^{-1}[B][K]^{-1}[L] \tag{16}$$

where $[I]$ is the identity matrix; $\bar{\lambda}=1/R$ represents the eigenvalue and $\{F\}$ the eigenvector.

The critical Rayleigh number for the onset of convection is given by $R_C=1/\bar{\lambda}_{max}$.

## 4. Results and discussion

### 4.1. The limiting case of an infinite layer

The limiting case $A\to\infty$ of the confined layer being the layer of infinite extent, results for this asymptotic situation are required to understand the effect of confinement and will be first given.

We start with the particular case where principal axes are in the $x$ and $y$ directions. The critical Rayleigh number is given in Fig. 2 as a function of the inversion parameter $\gamma$ for different permeability ratios, $K^*$, the angle $\theta$ being maintained at 0°. The scaling factor, $4/(1+K^{*1/2})^2$ reduces to unity for the isotropic case ($K^*=1$). With this normalization, results for various permeability ratios $K^*$ collapse toward a unique value $4\pi^2$ when $\gamma\gg 2$. We may notice in Eq. (2) that the quadratic term in $T$ becomes negligible when $\gamma$ becomes large and that $\gamma R$ becomes equivalent to the standard Rayleigh number, as shown in Eq. (8). With $\gamma$ decreasing below 2.0, a stable layer is formed near the upper boundary and a drastic decrease in $R_{mC}$ occurs, this decrease being related to the change in the definition of $R_m$, Eqs. (7a) and (7b). With $\gamma$ still decreasing, the constraining effect of the upper boundary is gradually reduced and becomes practically negligible at $\gamma\approx 1$. For the range $0<\gamma\leqslant 1$, $R_{mC}$ remains at the same value which is much below the one corresponding to classical convection ($\gamma\gg 2$). However, for this range, there is no collapse of the results into a single curve, although all individual curves corresponding to different $K^*$ lie nearby. Also, it is to be noted that replacing $K^*$ by $1/K^*$ does not change results since both extreme permeabilities $K_1$ and $K_2$ are involved with the same weight in the definition of the ordinate, $4R_{mC}/(1+K^{*1/2})^2$.

The critical wavelength $\lambda_{mC}$ for $\theta=0°$, which follows a trend comparable to the critical Rayleigh, is given in

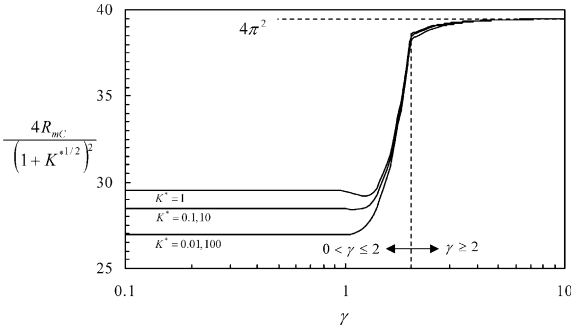


Fig. 2. Infinite layer: critical Rayleigh number $R_{mC}$ function of $\gamma$ and $K^*$ ($\theta=0°$).

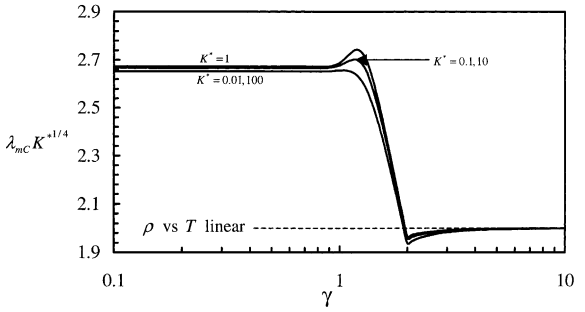


Fig. 3. Infinite layer: critical wavelength $\lambda_{mC}$ function of $\gamma$ and $K^*$ ($\theta = 0°$).

Fig. 3 as a function of $\gamma$ for $K^* = 1$, 0.1 and 0.01. With the scaling factor, $K^{*1/4}$, obtained from Tyvand and Storesletten's paper [6], the results collapse into a single curve for $\gamma \gg 2$. Elsewhere, the results will collapse for $K^*$ and $1/K^*$ (for instance, 0.1 and 10) but otherwise give rise to slightly different curves, according to a degree of anisotropy. With $\gamma$ decreasing below 2, $\lambda_{mC}$ encounters a drastic change and starts increasing suddenly. At $\gamma \leqslant 1$, the asymptotic behavior is reached for $\lambda_{mC}$, as it was the case for $R_{mC}$. A more detailed discussion of this situation where principal axes are in the $x$ and $y$ directions may be found in the article by Mahidjiba et al. [9].

The above discussion is now extended to an arbitrary orientation of the principal axes. Figs. 4 and 5 show respectively the critical Rayleigh number $R_{mC}$ and the critical wavelength $\lambda_{mC}$, as a function of $\gamma$ and $K^*$, for $\theta = 45°$. At this particular value of $\theta$, results for $K^*$ and $1/K^*$ again collapse on the same curves since case $1/K^*$ is the mirror image of case $K^*$. By contrast with Figs. 2 and 3, the asymptotic situation $\gamma \gg 2$ gives rise to different curves for $R_{mC}$ and $\lambda_{mC}$ according to the degree of anisotropy. This behavior concerning large $\gamma$ is in agreement with Tyvand and Storesletten results [6] for oblique axes.

The effect of $\theta$ on the incipient flow field at $\gamma = 0.5$ and $K^* = 0.1$ is shown in Fig. 6. For each $\theta$ in this figure,

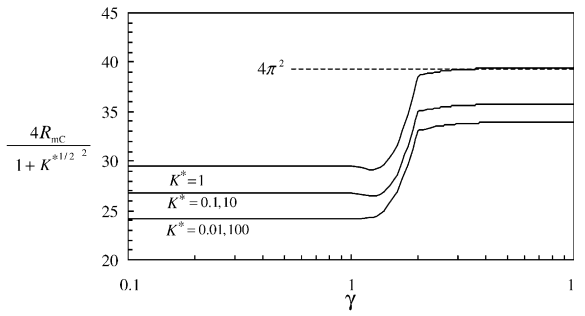


Fig. 4. Infinite layer: critical Rayleigh number $R_{mC}$ function of $\gamma$ and $K^*$ ($\theta = 45°$).

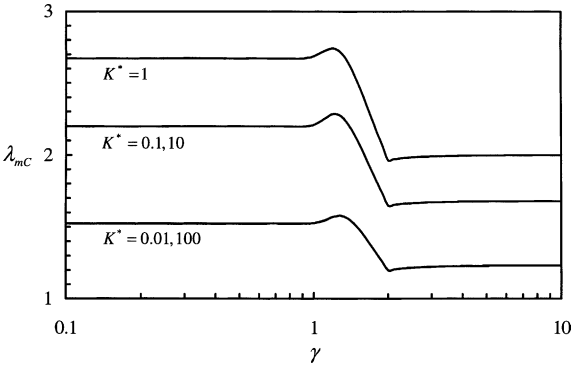


Fig. 5. Infinite wavelength $\lambda_{mC}$ function of $\gamma$ and $K^*$ ($\theta = 45°$).

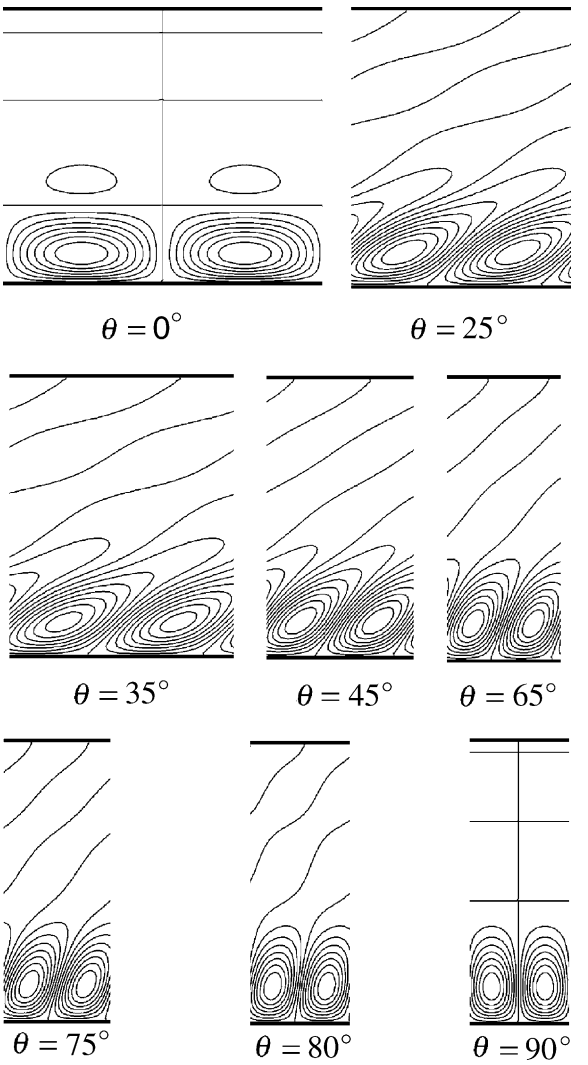


Fig. 6. Infinite layer: effect of the angle $\theta$ on the incipient flow ($\gamma = 0.5$; $K^* = 0.1$).

one wavelength of the infinite flow field is represented. For $\theta = 0°$ and 90°, secondary cells (above) are distinct from primary convection cells (bottom). For intermediate values of $\theta$, primary cells coalesce with secondary cells obliquely located, i.e., having their rotation in the same direction, with the result that only primary cells of elongated shape exist. The maximum intensity of motion within these elongated cells remains located near the lower boundary and the strength of the cells fades away in the upper direction.

### 4.2. The effect of confinement

Fig. 7 shows the influence of the aspect ratio $A_m$ on the critical Rayleigh number $R_{mC}$ for $\theta = 0°$ (or 90°) and $K^* = 0.1$. For reasons already mentioned previously concerning the scaling factor $4/(1 + K^{*1/2})^2$ used in the definition of the ordinate, it is worth recalling that $K^*$ may be changed for its reciprocal value $(1/K^*)$ without changing the value of the ordinate. If in addition, the scaling factor $K^{*1/4}$ is used in front of $A_m$, then results for a given value of $K^*$ or its reciprocal will fall on the same curve, for a given value of $\gamma$. Thus, curves given in Fig. 7 for $\gamma = 1000$, 2, 1.8 and 0.5 (or 1) are valid for $K^* = 0.1$ or 10. Finally from the above considerations, it may also be deduced that the curves of Fig. 7 also stand for $\theta = 90°$ provided that the label of the abscissa is changed for $A_m K^{*-1/4}$.

The upper curve $\gamma = 1000$ in Fig. 7 corresponds practically to the asymptotic case of a linear density–temperature relationship already studied by Mahidjiba et al. [8]. For $\gamma = 2$, the quadratic dependence in Eq. (1) introduces a slight discrepancy between curves $\gamma = 2$ and 1000. For $\gamma = 1.8$, the reduced influence of the upper boundary, due to the presence of an upper stable layer, results in a more pronounced reduction of the critical Rayleigh number. For $\gamma \leqslant 1$, an asymptotic situation is reached. As a consequence, results obtained for $\gamma = 1$ and 0.5 collapse on a single curve. All curves of Fig. 7 reach practically the asymptotic values of an infinite layer when $A_m K^{*1/4}$ $(\theta = 0°)$ or $A_m K^{*-1/4}$ $(\theta = 90°)$ is greater than ~5. For instance the curve $\gamma = 1.0$ (or 0.5) tends asymptotically to the value $4R_{mC}/(1 + K^{*1/2})^2 \approx 28.5$ given in Fig. 2 for $K^* = 0.1$. As described by Mahidjiba et al. [8], the minima for each of these curves are located at $A_{mC} = n\lambda_{mC}/2$ ($n$ being a positive integer) and $R_{mC}$ takes the value corresponding to an infinite layer. Elsewhere, the constraint of the vertical walls which imposes a given wavelength raises the value of $R_{mC}$. With increasing $A_m$, maxima (peaks) and minima are found to succeed one another, the maxima corresponding to the transition from $n$ to $n + 1$ convective cells.

Finally, it should be emphasized that each of the curves shown in Fig. 7 represents the lowest threshold beyond which motion occurs. The stability analysis described earlier provides other thresholds not represented on those curves. For instance, the part of the curve preceding the first peak, on each of the curves, stands for the threshold beyond which a single convective cell will appear in the cavity. That part of the curve could be extrapolated beyond the second peak at higher aspect ratios where it would still provide the threshold for a single convective cell. However, for aspect ratios between the first and second peaks, there exists a lower threshold corresponding to the occurrence of two convective cells. Fig. 8a and b show an enlarged view of the first two threshold values around the first peak, as obtained numerically, for $\gamma = 0.5$ and 1.8 respectively. The location where the two sets of points cross each other corresponds to the first peak.

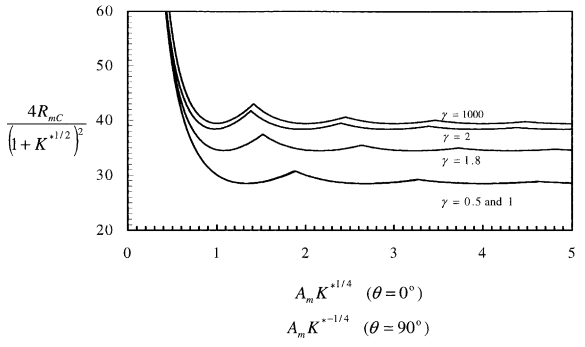


Fig. 7. Confined layer: effect of $A_m$ on $R_{mC}$ for various values of $\gamma$ ($\theta = 0°$; $K^* = 0.1$, 10).

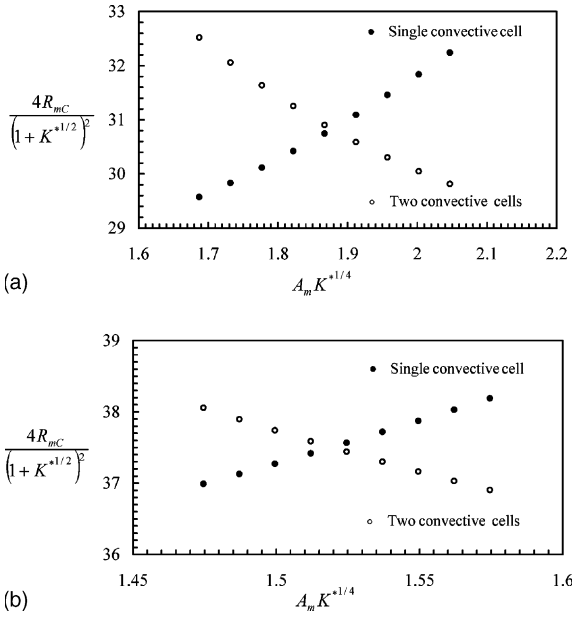


Fig. 8. Confined layer: effect of $A_m$ on the two first critical numbers corresponding to the two highest eigenvalues ($K^* = 0.1$, $\theta = 0°$): (a) $\gamma = 0.5$ and (b) $\gamma = 1.8$.

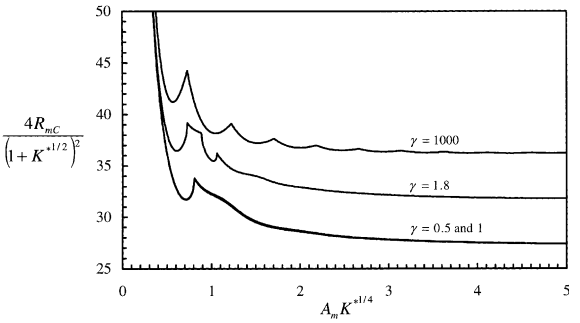


Fig. 9. Confined layer: effect of $A_m$ on $R_{mC}$ for various values of $\gamma$ ($\theta = 45°$, $K^* = 0.1$).

Fig. 9 shows the influence of the aspect ratio on the critical Rayleigh number for $K^* = 0.1$ and $\theta = 45°$. The same scale factors used for Fig. 7 are used here for the abscissa and the ordinate. Three curves corresponding to $\gamma = 1000$, 1.8 and 1.0 (or 0.5) are shown. Notable differences with Fig. 7 are observed, in particular concerning the two lower curves. We first consider the upper curve labeled $\gamma = 1000$ which represents the asymptotic case of a linear density–temperature relationship. The behavior of this curve was already discussed in the article by Mahidjiba et al. [8]. The asymptotic limit of an infinite layer $4R_{mC}/(1 + K^{*1/2})^2 \approx 35.8$ is practically reached at $A_m K^{*1/4} = 5$. That limit is slightly below $4\pi^2$ and corresponds to the results obtained by Tyvand and Storesletten [6]. With $A_m$ increasing from zero, the first minima are higher than the asymptotic limit and their spacing decreases slightly with $A_m$ increasing. This behavior is in contrast with the upper curve of Fig. 7. It is a consequence of the additional constraint imposed by the vertical boundaries when $\theta \neq 0°$ or 90°. The vertical walls, not only impose a given wavelength, but also modify the shape of the convective cells adjacent to them, as illustrated in Fig. 10. Without those walls, i.e., for the case of an infinite layer, all the cells are obliquely elongated and separated by oblique dividing streamlines.

Curves of Fig. 9 labeled $\gamma = 1.8$ and 1.0 (or 0.5) contrast with previous curves already described. They do not show multiple spaced peaks and, apart from a zcumbersome behavior observed for the range $\sim 0.7 < A_m K^{*1/4} <\sim 1.3$, in particular for curve $\gamma = 1.8$, both curves show a rather monotonous decrease towards the asymptotic value of an infinite layer, with $A_m K^{*1/4}$ increasing. This unusual behavior has to do with the particular way by which new convective cells are introduced in the layer when the aspect ratio is increased. By contrast will previous cases; new convective cells take place gradually. This particular behavior is related to the complete loss of symmetry characterizing the incipient flow fields when $\gamma < 2$ and $\theta \neq 0°$ (or 90°). Without the constraints of symmetry, new convective

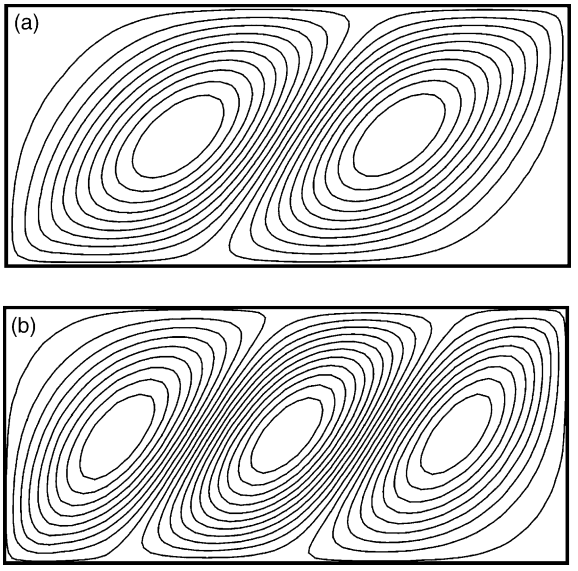


Fig. 10. Occurrence of a new convective cell "when centro-symmetry" prevails ($\gamma = 1000$, $\theta = 45°$ and $K^* = 0.1$): (a) $A_m K^{*1/4} = 1.21$ and (b) $A_m K^{*1/4} = 1.24$.

cells may be inserted smoothly with increasing aspect ratio. Incipient flow fields related to previous curves already discussed were subjected to two types of symmetry: one associated to $\gamma \gg 2$ and another one associated with $\theta = 0°$ or 90°. Those two types of symmetry are now discussed:

- *Symmetry with respect to the center of the cavity (centro-symmetry):* in classical convection ($\rho$ vs $T$ linear), asymptotically obtained when $\gamma \gg 2$, both upper and lower walls exert an equal influence on the incipient flow field with the result that a symmetry with respect to the center of the cavity ($x = 0$ and $y = 0$ in Fig. 2) or "centro-symmetry" prevails for any arbitrary $\theta$. This centro-symmetry is of the form

$$\Psi(-x,-y) = \Psi(x,y) \quad \text{(odd number of cells)} \tag{17a}$$

$$\Psi(-x,-y) = -\Psi(x,y) \quad \text{(even number of cells)} \tag{17b}$$

  When such a symmetry prevails, the occurrence of a new convective cell in the flow field necessitates a drastic rearrangement of all the existing cells, in their shape and relative strength, as illustrated in Fig. 10a and b, which shows incipient flow fields on each side of the second peak of Fig. 9, this peak being located at $A_m K^{*1/4} =\sim 1.22$ for $\gamma = 1000$.
- *Symmetry with respect to the vertical axis $x = 0$ (mirror-image symmetry):* For any arbitrary value $\gamma$, all flow fields with $\theta = 0°$ (or 90°) are symmetric with respect to a vertical axis dividing the cavity in two halves, according to

$$\Psi(-x,y) = \Psi(x,y) \quad \text{(odd number of cells)} \qquad (18a)$$

$$\Psi(-x,y) = -\Psi(x,y) \quad \text{(even number of cells)} \qquad (18b)$$

With that type of symmetry, all convective cells must have the same shape and intensity, so that the addition of a new cell also necessitates a drastic rearrangement of the flow field. This last case is illustrated in Fig. 11 where incipient flow fields are shown on each side of the second peak of Fig. 7, located at $A_{\mathrm{m}}K^{*1/4} \approx 3.27$ for $\gamma = 1$ (or 0.5).

The constraints associated to symmetries Eqs. (17a), (17b), (18a) and (18b) produce eigenvalues (or their reciprocal, $R_{\mathrm{mC}}$) of the type shown in Fig. 8, near a given peak. These constraints do not apply to the two lower curves of Fig. 9. Fig. 12 gives the evolution, with $A_{\mathrm{m}}$ increasing, of the largest eigenvalues associated with the peculiar behavior of those curves for the range $\sim 0.6 < A_{\mathrm{m}}K^{*1/4} <\sim 1.0$. Fig. 13 illustrates the progressive way by which new convective cells are introduced in the flow field, near the lower boundary, in the absence of any symmetry.

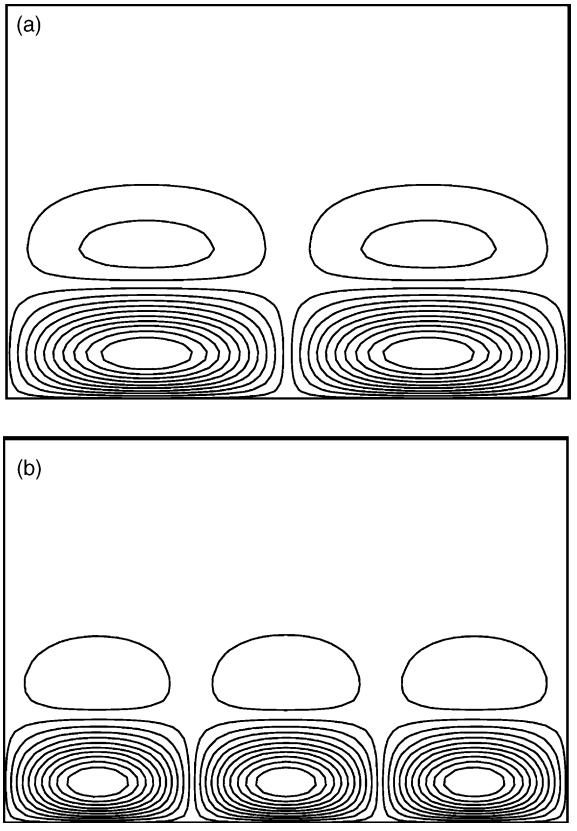


Fig. 11. Occurrence of a new convective cell "when mirror-image symmetry" prevails $\gamma = 0.5$, ($\theta = 45°$ and $K^* = 0.1$): (a) $A_{\mathrm{m}}K^{*1/4} = 3.25$ and (b) $A_{\mathrm{m}}K^{*1/4} = 3.30$.

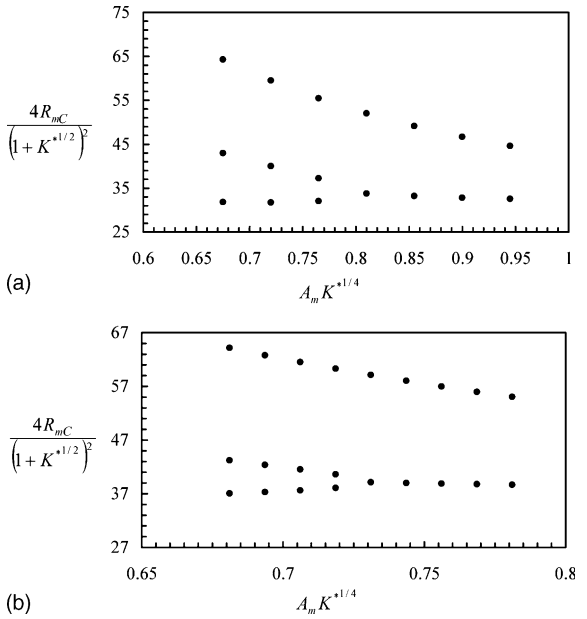


Fig. 12. Confined layer: effect of $A_{\mathrm{m}}$ on $R_{\mathrm{mC}}$ ($K^* = 0.1$, $\theta = 45°$): (a) $\gamma = 0.5$ and (b) $\gamma = 1.8$.

## 5. Conclusion

A stability study has been performed for the case of a horizontal anisotropic porous layer of finite/infinite lateral extent, saturated with water in the presence of the density extremum at 4 °C. Critical Rayleigh numbers have been obtained, functions of the aspect ratio, the permeability ratio, the orientation angle of the principal axes and the inversion parameter, this last one defining the vertical position of the density extremum in pure conduction. Results have been brought to a simple form by the use of particular definitions of the Rayleigh number and the aspect ratio, based on the thickness of the unstable layer and on the difference of temperature across that layer.

Results concerning the infinite layer, having a density extremum between the upper and lower boundaries and with oblique principal axes, reveal that primary convective cells near the lower boundary coalesce with upper secondary cells to form obliquely elongated convective cells evenly distributed. When the layer is limited by vertical boundaries, the symmetry conditions, which prevail, either in classical convection or when the principal axes are vertically/horizontally oriented, disappear when the maximum density lies between the upper and lower boundaries and the principal axes are arbitrary oriented. The consequence is a progressive evolution, without drastic change of the incipient flow field, with increasing aspect ratio, new cells being in-

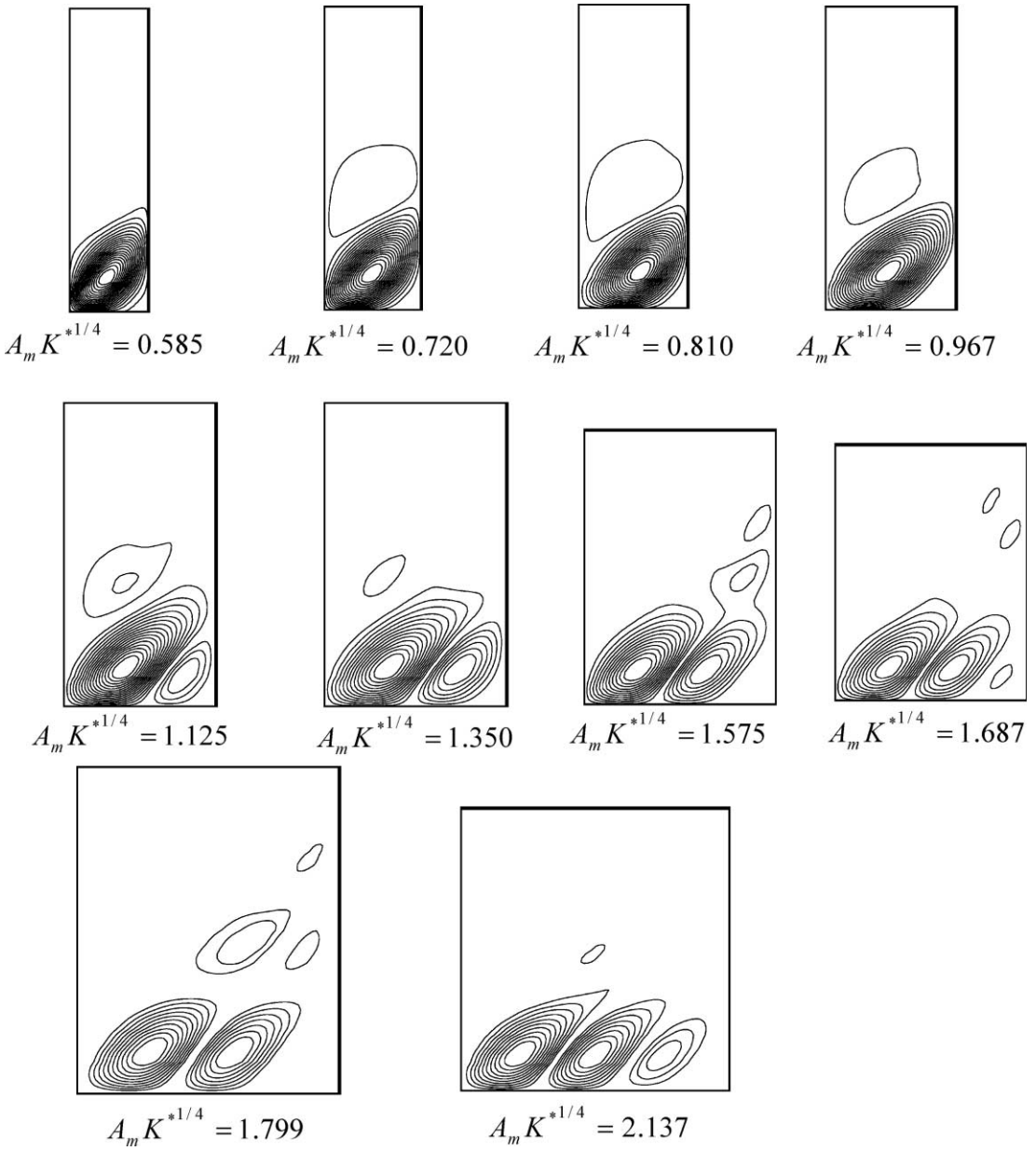


Fig. 13. Occurrence of a new cell when no symmetry is involved ($\gamma = 0.5$ , $\theta = 45°$ and $K^* = 0.1$).

troduced smoothly, and critical Rayleigh decreasing monotonously i.e., without multiple peaks, toward the asymptotic value of an infinite layer.

## Acknowledgements

This research was financially supported by the Natural Science and Engineering Council of Canada and FCAR of Province of Quebec.

## References

[1] G. Veronis, Penetrative convection, Astrophy. J. 137 (1963) 641–663.
[2] S. Musman, Penetrative convection, J. Fluid Mech. 31 (1968) 343–360.
[3] D.R. Moore, N.O. Weiss, Nonlinear penetrative convection, J. Fluid Mech. 61 (1973) 553–581.
[4] D. Poulikakos, Onset of convection in a horizontal porous layer saturated by cold water, Int. J. Heat Mass Transfer 28 (1985) 1899–1905.

[5] M. Mamou, P. Vasseur, L. Robillard, Thermoconvective instability in a horizontal porous cavity saturated with cold water, Int. Commun. Heat Mass Transfer 42 (1999) 4487–4500.
[6] P.A. Tyvand, L. Storesletten, Onset of convection in an anisotropic porous medium with oblique principal axes, J. Fluid Mech. 226 (1991) 371–382.
[7] B. Straughan, D.W. Walker, Anisotropic porous penetrative convection, Proc. R. Soc. Lond. A 452 (1996) 97–115.
[8] A. Mahidjiba, L. Robillard, P. Vasseur, M. Mamou, Onset of convection in an anisotropic porous layer of finite lateral extent, Int. Commun. Heat Mass Transfer 27 (2) (2000) 333–342.
[9] A. Mahidjiba, L. Robillard, P. Vasseur, Onset of convection in a horizontal anisotropic Porous layer saturated with water near 4 °C, Int. Commun. Heat Mass Transfer 27 (6) (2000) 765–774.
[10] L. Robillard, P. Vasseur, Convective response of a Mass of water near 4 °C to a constant cooling rate applied on its boundaries, J. Fluid Mech. 16 (1982) 199–207.